Chapter

Synthesis and Investigation of the Physical Properties of Lead-Free BCZT Ceramics

Dang Anh Tuan, Vo Thanh Tung, Le Tran Uyen Tu and Truong Van Chuong

Abstract

This work presents the structure, microstructure, and physical properties of low sintering temperature lead-free ceramics $0.52(Ba_{0.7}Ca_{0.3})TiO_3$-$0.48Ba(Zr_{0.2}Ti_{0.8})O_3$ doped with nano-sized ZnO particles (noted as BCZT/x, x is the content of ZnO nanoparticles in wt.%, x = 0.00, 0.05, 0.10, 0.15, 0.20, and 0.25). The obtained results of Raman scattering and dielectric measurements have confirmed that Zn^{2+} has occupied B-site, to cause a deformation in the ABO_3-type lattice of the BCZT/x specimens. The 0.15 wt.% ZnO-modified ceramic sintered at 1350°C exhibited excellent piezoelectric parameters: d_{33} = 420 pC/N, d_{31} = −174 pC/N, k_p = 0.483, k_t = 0.423, and k_{33} = 0.571. The obtained results indicate that the high-quality lead-free BCZT ceramic could be successfully synthesized at a low sintering temperature of 1350°C with an addition of appropriated amount of ZnO nanoparticles. This work also reports the influence of the sintering temperature on structure, microstructure, and piezoelectric properties of BCZT/0.15 compound. By rising sintering temperature, the piezoelectric behaviors were improved and rose up to the best parameters at a sintering temperature of 1450°C (d_{33} = 576 pC/N and k_p = 0.55). The corresponding properties of undoped BCZT ceramics were investigated as a comparison. It also presented that the sintering behavior and piezo-parameters of doped BCZT samples are better than the undoped BCZT samples at each sintering temperature.

Keywords: lead-free, BZT-BCT, ceramics, nanoparticle, ZnO

1. Introduction

Perovskite ABO_3-type compounds with high flexibility in symmetry play an important role in materials science. Typical materials such as lead zirconate titanate (PZT) based on family $BaTiO_3$ have received a lot of attention due to their outstanding dielectric, ferroelectric, and piezoelectric performance.

Nevertheless, PZT systems are globally restricted due to evaporating toxic lead oxide to the environment during preparation. With the recent growing demand of global environmental and human health protection, many non-lead materials have been systematically studied to replace the lead-based ceramics [1, 2].

In 2009, based on alternating with A- and/or B-sites in perovskite $BaTiO_3$, Liu and Ren established a new lead-free ferroelectric system $Ba(Zr_{0.2}Ti_{0.8})O_3$-$x(Ba_{0.7}Ca_{0.3})$

TiO_3 (abbreviated as BZT-BCT) that has excellent piezoelectricity (d_{33} = 620 pC/N at x = 50, i.e., morphotropic phase boundary or MPB composition) [3]. After that the BZT-BCT materials have been widely studied [4–6]. It is noted that based $BaTiO_3$ ceramics have been usually sintered at a very high temperature to obtain the desired properties [7–9] which causes many difficulties in the preparation and application of these materials. It is well-known that sintering behavior can be improved by using nanostructured raw materials and/or sintering aids [10, 11]. Among commonly used dopants, ZnO (in nano- or microscale) is known as an effective sintering aid for enhancing density and electric properties of piezoceramics [12–14].

In this work, the effects of ZnO nanoparticles as well as sintering temperature on structure, microstructure, and some electric properties of $0.48Ba(Zr_{0.2}Ti_{0.8})O_3$-$0.52(Ba_{0.7}Ca_{0.3})TiO_3$ or BCZT composition were detailedly presented.

2. Experimental produces

2.1 Preparing ZnO nanoparticles

ZnO nanoparticles were synthesized using zinc acetate and ammonia solutions as initial materials. Accordingly, zinc acetate was dissolved in distilled water to form solution. Then NH_4OH solution was gradually dropped into zinc acetate solution and stirred until a white precipitate was received. The amount of NH_4OH was enough so that the overall reaction to form ZnO is as follows [15]:

$$(CH_3COO)_2Zn + 2NH_4OH \rightarrow ZnO + 2(CH_3COO)NH_4 + H_2O.$$

The obtained white precipitate was filtered and washed several times with the aid of vacuum filter machine and then annealed at a temperature of 250°C for 1 h to remove unwanted products.

Figure 1 shows XRD and microstructure image (measured by D8 Advance, Bruker AXS, and Nova NanoSEM 450-FEI, respectively) of the obtained ZnO powder after annealing at 250°C for 1 h.

Detailed structural characterization demonstrated that the synthesized product possesses pure hexagonal symmetry [16]. The obtained ZnO particles are spherical in shape with their average diameter of 59 nm (according to Scherrer equation). The nanostructured ZnO powder was used as a sintering aid in fabrication of BCZT ceramics.

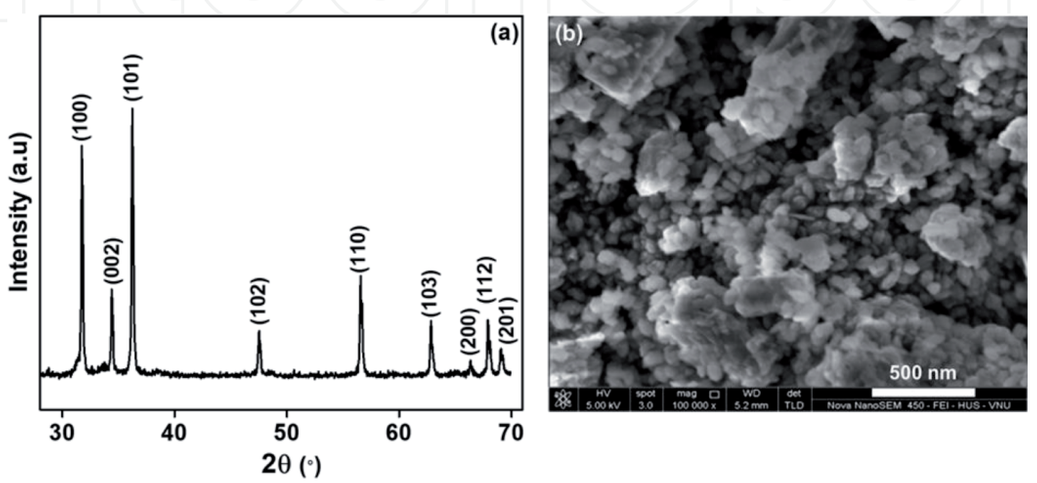

Figure 1.
(a) X-ray diffraction (XRD) and (b) micrograph of as-prepared ZnO powder.

2.2 Fabrication of ZnO nanoparticles doped BCZT ceramics at low sintering temperature

A conventional ceramic fabrication technique was used to prepare lead-free ceramics $0.52(Ba_{0.7}Ca_{0.3})TiO_3$-$0.48Ba(Zr_{0.2}Ti_{0.8})O_3$ doped with ZnO nanoparticles (abbreviated as BCZT/x, x is the content of ZnO in wt.%, x = 0.00, 0.05, 0.10, 0.15, 0.20, 0.25). The raw materials with high purity (>99%) of $BaCO_3$, $CaCO_3$, ZrO_2, and TiO_2 (Merck) were weighed and mixed in a planetary milling machine (PM400/2-MA-Type) using ethanol as a medium for 20 h. The obtained powders were calcined at 1250°C for 3 h. The calcined powder was milled again in ethanol for 20 h; after that the x wt.% of ZnO nanoparticles were added, finely mixed, and then pressed into desired-shape specimens by uniaxial pressing with a pressure of 100 MPa. Sintering was carried out at various temperatures for 4 h. The X-ray diffraction patterns were recorded at room temperature by a D8 Advance, Bruker AXS. The tetragonal and rhombohedral volume fractions, τ_T and τ_R, were, respectively, evaluated using the equations below [17]:

$$\tau_T = \frac{I_{200}^T + I_{002}^T}{I_{200}^T + I_{200}^R + I_{002}^T}, \tag{1}$$

$$\tau_R = \frac{I_{200}^R}{I_{200}^T + I_{200}^R + I_{002}^T}, \tag{2}$$

where $I_{200/002}^{T/R}$ are the corresponding tetragonal (T) and rhombohedral (R) peak intensities.

The crystalline structure and lattice parameters of all samples were estimated from fitting results of the XRD data by using the Powder Cell software [18]. The surface of the sintered samples was processed and cleaned by an ultrasonic cleaner and then observed by scanning electron microscopy (SEM, Nova NanoSEM 450-FEI). Particle size is the mean linear intercept length that was determined using an intercept method with the assistance of Lince software [19]. The silver pastes were fired at 450°C for 30 minutes on both sides of these sintered bulks as electrodes for electrical measurements. Dielectric properties of the materials were determined together using an impedance analyzer (Agilent 4396B, Agilent Technologies, America, HIOKI3532) by measuring the capacitance of the specimens from room temperature to 120°C. Raman scattering spectra was measured using LabRAM-1B (Horiba Jobin Yvon). Ferroelectricity was studied by using the Sawyer-Tower circuit method. In order to study piezoelectric properties, the samples were polled in silicon oil bath by applying the DC electric field of 2 kV/mm for 60 minutes at room temperature. The main piezoelectric parameters were calculated when using a resonance method (Agilent 4396B, HP4193A) and all formulas in the IEEE standard for piezoelectric ceramic characterization [20].

3. Results and discussion

3.1 Structure, microstructure, and electric properties of BCZT/x ceramics sintered at temperature of 1350°C

Figure 2(a) shows X-ray diffraction patterns of the BCZT/x ceramics at various contents of ZnO nanoparticles measured at room temperature. All the compositions have demonstrated pure perovskite phases, and no trace of secondary phase was

detected in the investigated region. **Figure 2(b)** plots the enlarged XRD patterns in the range of (44–46)° of BCZT/x ceramics. As shown, all BCZT/x ceramics have tetragonal symmetry (space group P4mm) characterized by splitting (002)/(200) peaks at around 2θ of 45° with the intensity changing between samples. Moreover, the position of these diffraction peaks shifted to lower angles as increasing x.

Figure 3 illustrates the variation in the lattice parameters, (a, c), and tetragonality, c/a, as a function of the addition of ZnO nanoparticles, x, for BCZT/x ceramics sintered at 1350°C. As increasing x, constant (a) increases significantly, whereas constant (c) and tetragonality (c/a) reach their maximum values at x = 0.15 wt.%. It likely indicated that Zn^{2+} ions were incorporated into the BCZT lattices, and a stable solid solution was formed in the ceramics. However, Zn^{2+} ions did not change crystal symmetry of the materials that only varied the size of unit cells. Considering the radii of Ba^{2+}, Ca^{2+}, Ti^{4+}, Zr^{4+}, O^{2-}, and Zn^{2+} of 1.44, 1.34, 0.605, 0.79, 1.4, and 0.74 Å, respectively, Zn^{2+} is possibly substituted for the B-site at (Ti^{4+}, Zr^{4+}) positions within ABO_3 perovskite structure that induced a lattice distortion in the BCZT/x ceramics. This result would cause the diffuse transition behavior in the materials and will be detailedly discussed in following section.

Surface morphologies of the BCZT/x ceramics sintered at 1350°C are shown in **Figure 4**.

It is evident that addition of nanostructured ZnO has strongly influenced the microstructure. Clean surfaces were observed for BCZT/*x* samples with

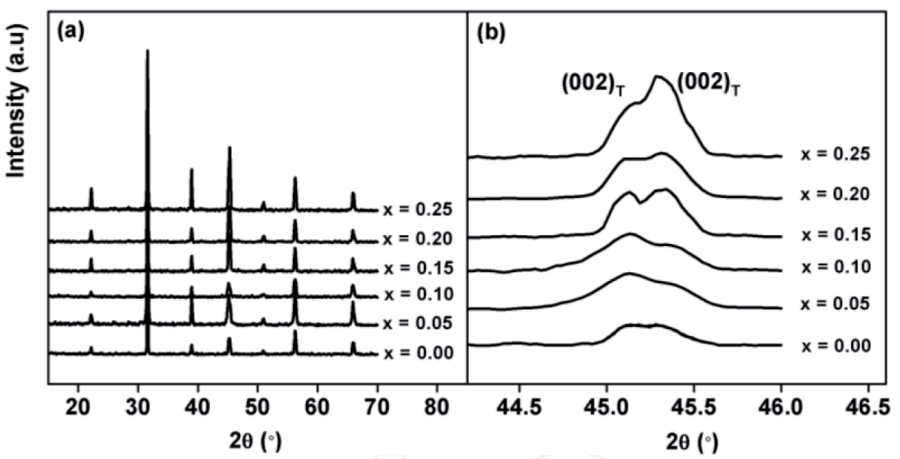

Figure 2.
XRD patterns (a) and expanded XRD patterns in the 2θ range of (44–46)° and (b) of the BCZT/x ceramics sintered at temperature of 1350°C.

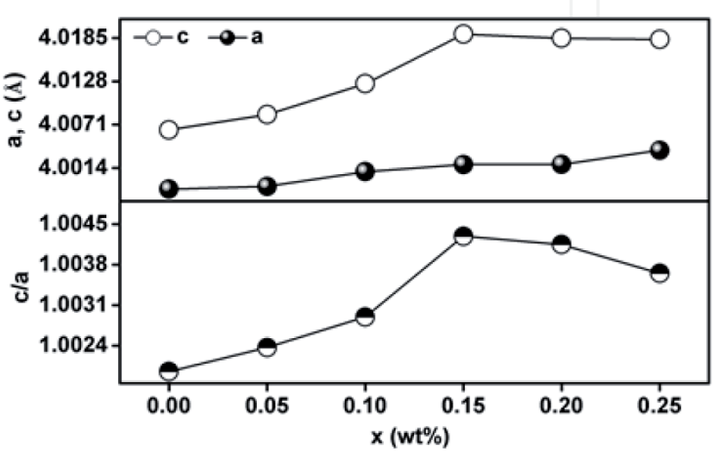

Figure 3.
Lattice parameters and tetragonality for the BCZT/x ceramics.

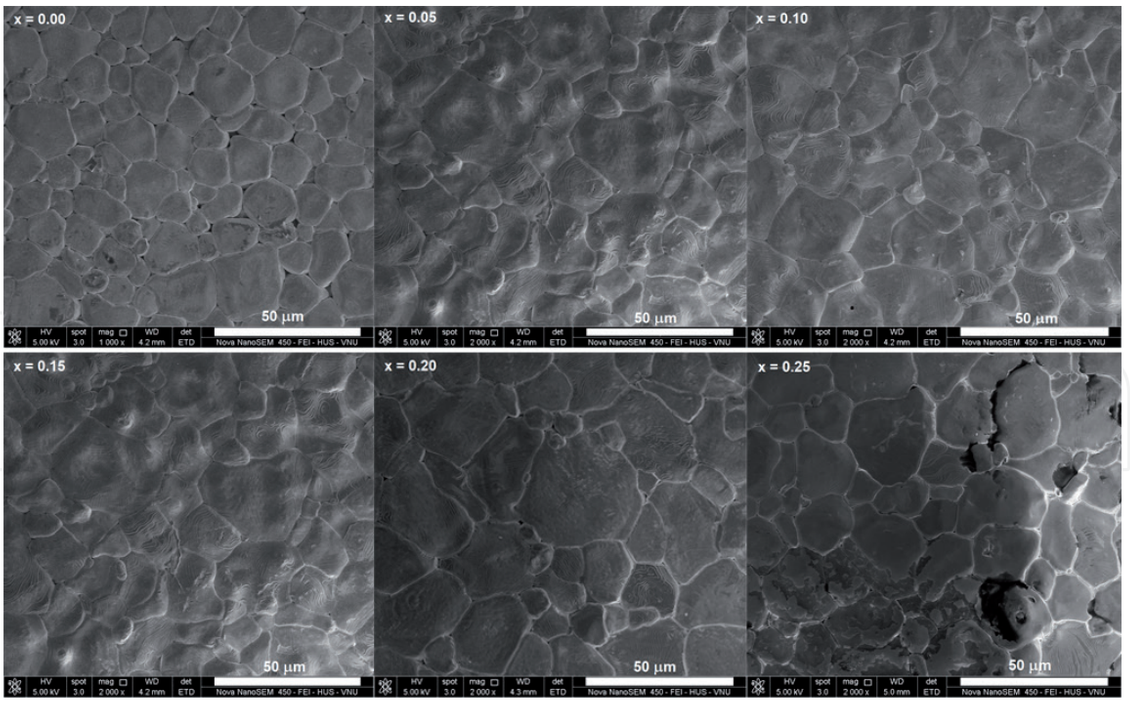

Figure 4.
SEM images of the BCZT/x ceramics sintered at 1350°C.

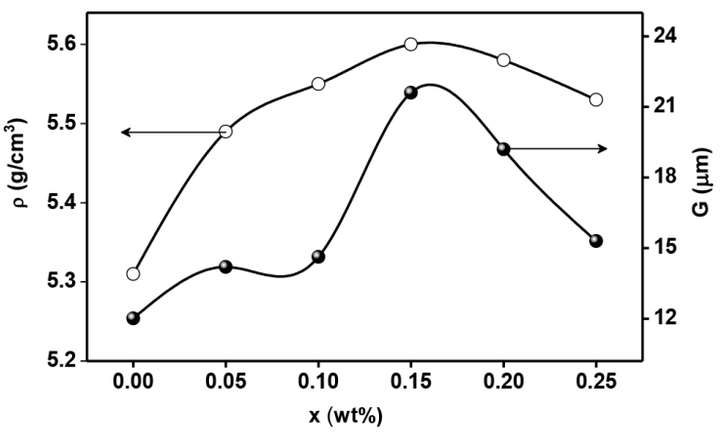

Figure 5.
Dependence of grain size, G, and density, ρ, on the ZnO nanoparticle content.

x = 0.00–0.15, and the grain size raised and reached the maximum value of 21.6 μm at x = 0.15 compound. The liquid phase, however, appeared on the grain surface and boundary as x > 0.15. It may be an excess amount of nano-sized ZnO particles during sintering, accumulating at the surface and grain boundary to restrict grain size evolution. Therefore, the experimental results indicate that solubility limit of ZnO nanoparticles in BCZT substrate is below 0.15 wt.% at a sintered temperature of 1350°C. Dependence of grain size and density on the ZnO nanoparticle content is in the same manner (**Figure 5**). Thus, the BCZT/0.15 composition was expected to possess excellent electric properties.

Figure 6 illustrates temperature dependences of permittivity, ε(T), of the BCZT/x ceramics measured with frequency of 1 kHz at room temperature. It is clear to see that the samples with ZnO addition exhibit a typical temperature dependence of permittivity. A wide cubic-tetragonal phase transition at the temperature around 70°C was observed for all samples. Furthermore, another phase transition was found around 40°C for BCZT/0.00 composition (without ZnO nanoparticles) that is in the MPB region of BCZT and seems to be related to a tetragonal-rhombohedral

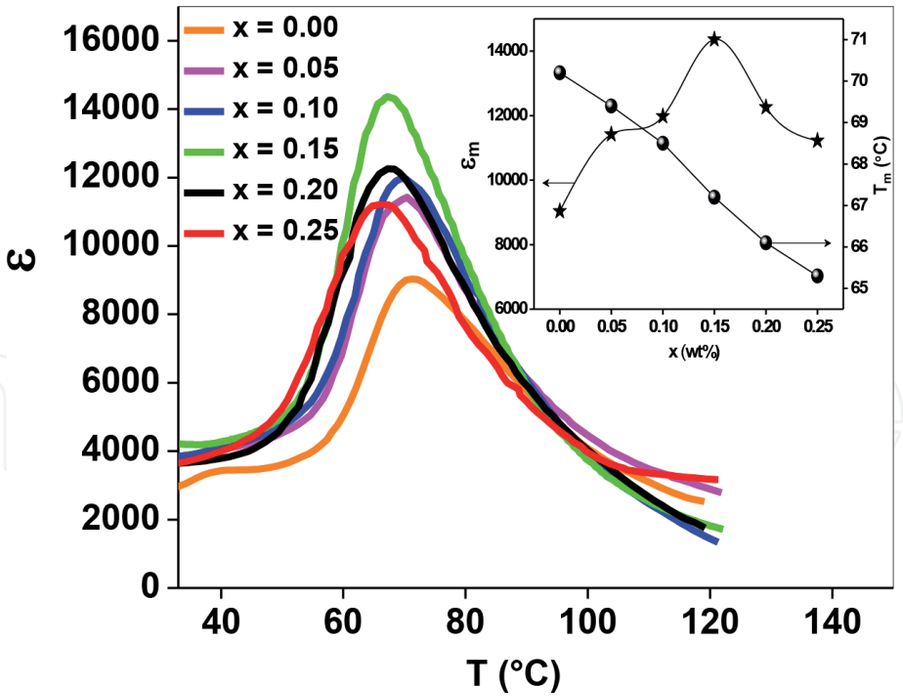

Figure 6.
Plot of permittivity versus temperature measured at 1 kHz for BCZT/x systems.

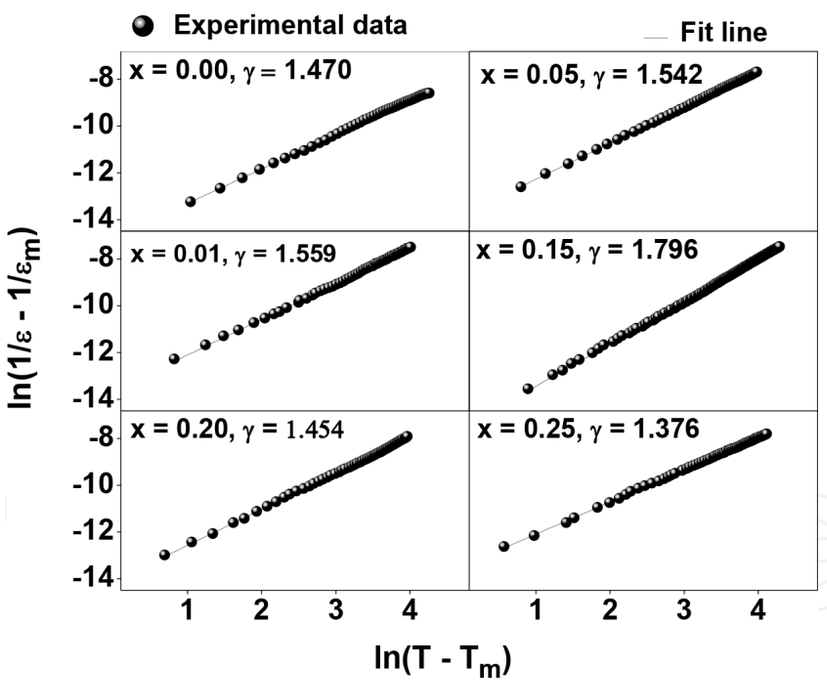

Figure 7.
$\ln(1/\varepsilon - 1/\varepsilon_m)$ versus $\ln(T - T_m)$ for BCZT/x systems.

phase transition as reported in the literatures [3, 21]. It is supposed that a part of the material has changed into rhombohedral phase with small amount so that this phase was not identified in X-ray patterns but can be observed in ε(T) curve. The mentioned phase transition was disappeared as raising content of ZnO nanoparticles. It may be shifted to lower temperature. It can be seen that ZnO nanoparticles have strongly affected dielectric properties. First, the shape of permittivity-temperature curves of the ZnO-added samples is broadened and shifted toward the lower-temperature region. This is due to the lattice distortion and indicates the ferroelectric diffuse transitions as reported in the literature [22]. The highest permittivity of

the samples, ε_m, nonlinearly depends on ZnO content. It increases with increasing ZnO content, reaches a maximal value of 14,361 for the BCZT/0.15 composition, and decreases monotonously after that. The temperature T_m corresponding to the maximum permittivity, ε_m, reduces with the increase of ZnO concentration due to the lattice distortion, as shown in XRD patterns. **Figure 7** presents the plots of $\ln(1/\varepsilon - 1/\varepsilon_m)$ versus $\ln(T - T_m)$ measured at 1 kHz for the BCZT/x ceramic that was fitted with modified Curie-Weiss law to obtain diffuseness degree parameter, γ. It can be observed that γ was changed as a function of x and reached the highest value of 1.796 at x = 0.15 composition.

As mentioned above, the diffuse characterization of BCZT/x ceramics may be a result of replacing Zn^{2+} for B-site ion (Ti^{4+}, Zr^{4+}). To put it more clearly, the room temperature Raman spectrum of the BCZT/x ceramics was recorded and analyzed (**Figure 8**). As shown, Raman modes of $BaTiO_3$-based systems are named as A_1(TO1), A_1(TO2), E(TO2), A_1(TO3), and A_1(LO3)/E(LO3) in the range of 150–1000 cm^{-1} [6]. The position and half-width of these modes were determined by fitting Raman data with Lorentzian function. E(TO2) vibration mode that has been associated with the tetragonal-cubic phase transition shifted to a lower wavenumber (**Figure 9(a)**). It means that substitution for B-site by Zn^{2+} results in reducing average B-O bonding energies. Thus, tetragonal-cubic

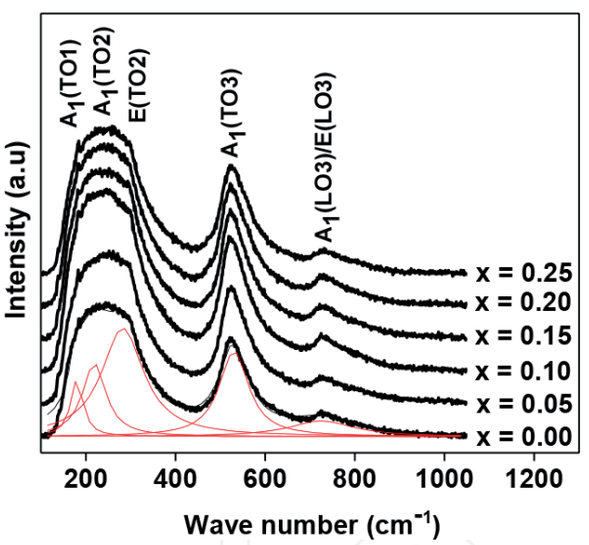

Figure 8.
Raman spectrum of BCZT/x systems recorded at room temperature.

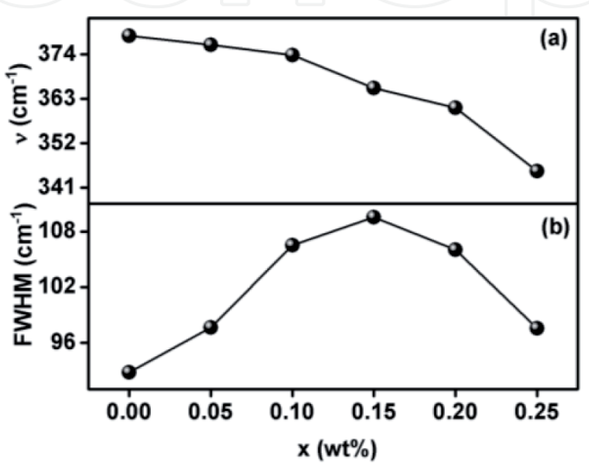

Figure 9.
(a) Raman shift, ν, of E(TO2) and (b) half-width, FWHM, of A_1(TO2) as a function of ZnO nanoparticles, x.

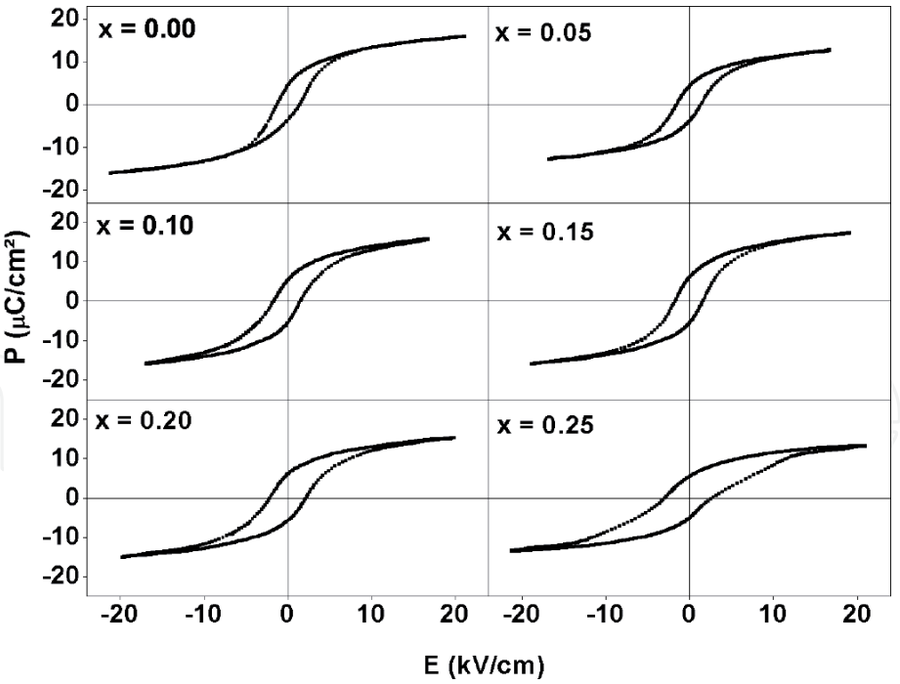

Figure 10.
Ferroelectric (P-E) hysteresis loops of BCZT/x systems.

phase transition temperature was diminished (see inset in **Figure 6**). The A_1(TO2) vibration mode was considered as the most sensitive to the lattice distortion that can be evaluated by FWHM of A_1(TO2) as presented in **Figure 9(b)**. It has been shown that FWHM depends on ZnO content and reached a maximum value at x = 0.15. It means the material sample added with 0.15 wt.% of ZnO has shown the highest disorder [23]. In other words, FWHM of the Raman mode A_1(TO2) also reflects the diffuseness of the ferroelectric-paraelectric phase transition as diffuseness degree. This obtained result is well appropriated with the result given from the temperature dependence of permittivity as presented in **Figure 6** where we can see that the diffuseness degree, γ, reached a maximum value for the same ZnO content x = 0.15 (see **Figure 7**).

Figure 10 presents P-E relationships for BCZT/x ceramics measured at room temperature. Received hysteresis loops were well saturated and fairly slim for all samples that assert again diffuse ferroelectric nature in BCZT/x ceramics. The characterized values of remanent polarization, P_r, and coercive field, E_c, depended on ZnO nanoparticles concentration as illustrated in **Figure 11**. As shown, when x content varied in the region of 0.00–0.25, P_r increased and reached a maximum value of 6.19 μC/cm^2 at x = 0.15 and then decreased monotonously. This result could be explained based on an amelioration in microstructure [24]. According to that, poor ferroelectricity was received at grain boundary. Thus, polarization of grain boundary may be very small or zero. Alternatively, space charges eliminate polarization charge from grain surface that depletion layer can be established. That caused polarization interruption on particle surface to form depolarization field which lowers polarization. The reduced number of grain boundary is due to increasing grain size that could be the reason for raising remanent polarization and vice versa. In this study, the grain size, G, of these ceramics was controlled by varying doping concentration of nano-sized ZnO particles as shown in **Figure 5**. The dependence of coercive field on ZnO nanoparticles content shows that the parameter continuously intensified in the range of (1.36–2.72) kV/cm as raising x. In other words, ZnO nanoparticles made the ceramics harder. The enhancement of E_c value could be due to the increase of charged oxygen vacancies as doping that pinned to the movement

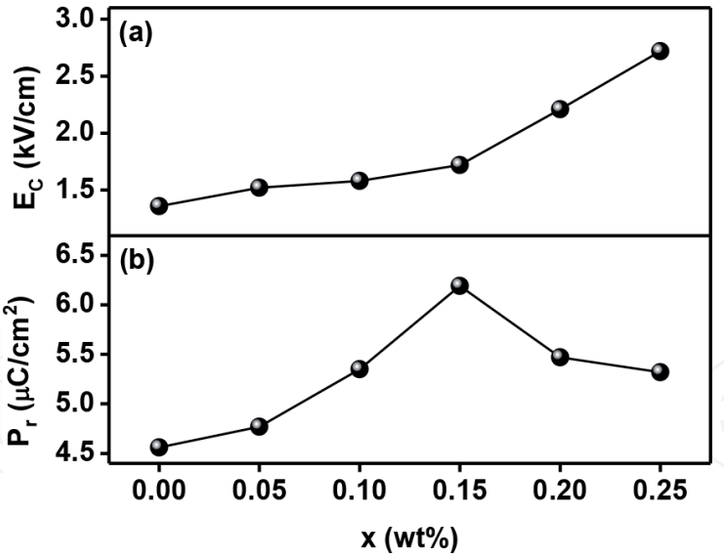

Figure 11.
Values of E_c and P_r as a function of x.

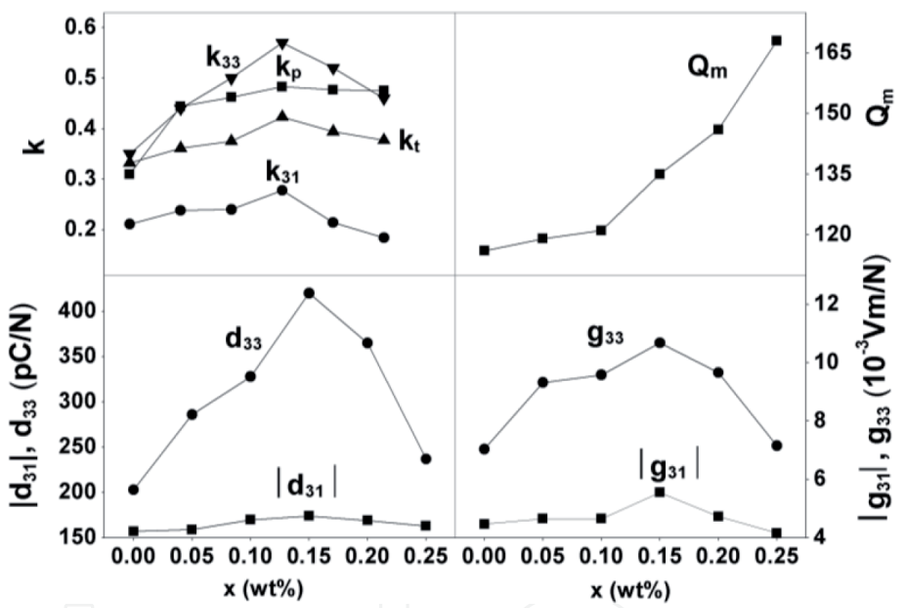

Figure 12.
Nano-sized ZnO content dependence of some piezo-parameters for BCZT/x ceramics.

of ferroelectric domain walls. The obtained values of E_c demonstrated that the BCZT/x materials are typically soft compared to electric properties.

Figure 12 displays the electromechanical coupling factor (k), piezoelectric constant (d_{33}, d_{31}, g_{33}, g_{31}), and mechanical quality factor (Q_m) with various amounts of ZnO nanoparticles.

It can be observed that k, g_{33}, g_{31}, d_{33}, and d_{31} curves possess maximum values for the BCZT/0.15 compound as presented in **Table 1**.

As mentioned above, the comprehensive analysis of X-ray diffraction, SEM images, and dielectric properties have proven the ZnO addition induced lattice distortion. The degree of this local lattice distortion increased up to the maximal value as ZnO concentration raised up to 0.15 wt.%. It is supposed the spontaneous polarization in each nano-domain has contributed to overall spontaneous polarization that enhanced piezoelectric characteristics of the material samples. Beyond the value of 0.15, the piezoelectric parameters decrease due to residual amount of ZnO nanoparticles agglomerating at the surface and grain boundary restricting

k_p	k_t	k_{31}	k_{33}	d_{33} (pC/N)	d_{31} (pC/N)	g_{33} (10^{-3} V m/N)	g_{31} (10^{-3} V m/N)
0.483	0.423	0.278	0.571	420	−174	10.68	−5.55

Table 1.
Values of coupling factors (k_p, k_t, k_{31}, k_{33}) and piezoelectric constants (d_{31}, d_{33}, g_{31}, g_{33}) of BCZT/0.15 sample sintered at 1350°C.

grain size growth. According to Ying-Chieh Lee et al., Zn^{2+} is substituted into the B-site to generate a doubly oxygen vacancy for compensation [12]. The presence of charged oxygen vacancies would be pinned by the movement of ferroelectric domain walls and consequently to enhance the Q_m value. The result is similar to that reported by Jiagang Wu et al., who used micro-size ZnO as an acceptor for the $Ba_{0.85}Ca_{0.15}Ti_{0.90}Zr_{0.10}O_3$ ceramic sintered at 1450°C [25].

3.2 Influence of sintering temperature on structure, microstructure, and piezoelectric properties of doped BCZT ceramics

In this section, effects of sintering temperature on the structure, microstructure, and piezoelectric properties of 0.15 wt.% modified BCZT or BCZT/0.15 compound are presented.

Figure 13 shows XRD patterns of BCZT/0.15 ceramic sintered at various temperatures of 1300, 1350, 1400, and 1450°C. All samples exhibited a pure perovskite phase, and no second-phase trace was detected in the investigated region. To study the effect of the sintering temperatures on the structure of BCZT/0.15 material, enlarged XRD patterns in the range of (44–46)° corresponded to each sintering temperature were analyzed by fitting XRD data with Gaussian function (inset in **Figure 13**). As shown, there were splitting (200)/(002) diffraction peaks at around 2θ of 45° for specimens sintered at 1300, 1350, and 1400°C, which means these samples have tetragonal symmetry. However, coexistence of rhombohedral and tetragonal phases was observed for the sample sintered at 1450°C in which tetragonal volume fraction, calculated by using Eq. (1), was 67.3%. In other words, BCZT/0.15 sample sintered at 1450°C could be MPB composition. Mixture of tetragonal-rhombohedral phases was also observed for BCZT/0.00 specimen (without ZnO nanoparticles) sintered at 1450°C (**Figure 14**) in which tetragonal volume

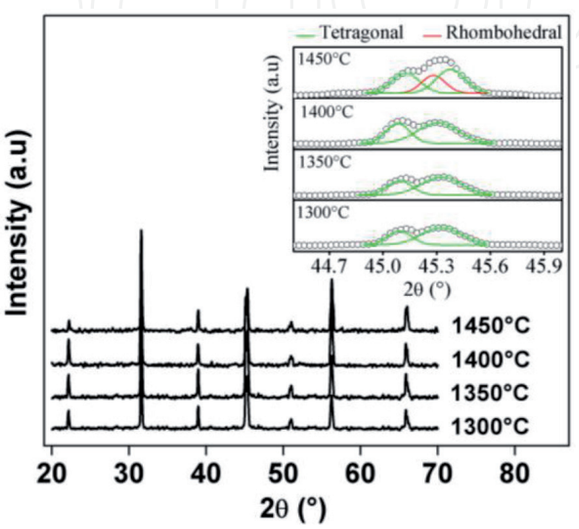

Figure 13.
XRD patterns of BCZT/0.15 sintered at different temperatures.

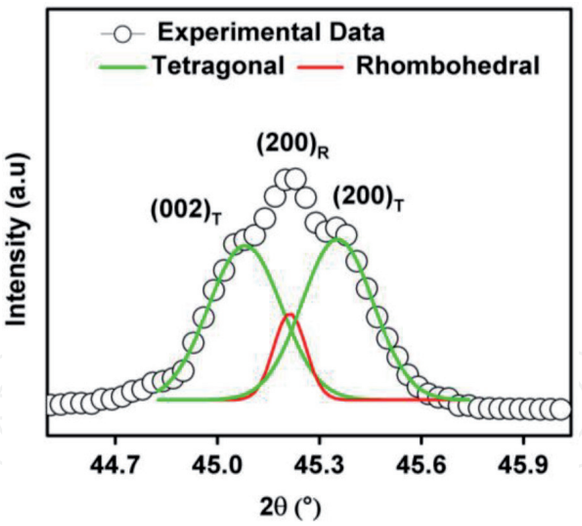

Figure 14.
Expanded XRD in the region of (44–46)° for BCZT/0.00 composition [26].

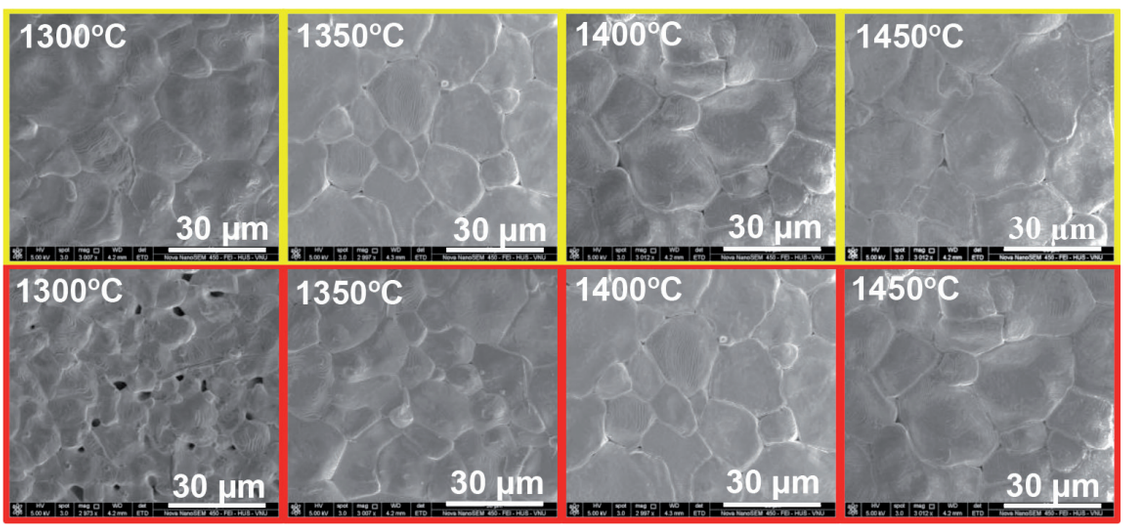

Figure 15.
SEM images of BCZT/0.15 (yellow border) and BCZT/0.00 (red border) ceramics sintered at various temperatures.

fraction was 71.7% [26]. It could be concluded that ZnO nanoparticle content of 0.15 wt.% did not change crystalline symmetry but only varied the fraction of phases in the samples. This could affect the piezoelectric properties of BCZT/0.00 and BCZT/0.15 samples sintered at 1450°C.

Figure 15 illustrates surface morphologies of BCZT/0.00 and BCZT/0.15 materials sintered at various temperatures. Grain size and density were calculated and listed in **Table 2**.

Porous microstructure with small grains was received for BCZT/0.00 ceramic sintered at 1300°C (**Figure 15**). However, when 0.15 wt.% of ZnO nanoparticle content was added, a denser microstructure with larger particles is viewed at the same sintering temperature. Moreover, both grain size and density of BCZT/0.00 and BCZT/0.15 samples were raised as sintering temperature increased (**Figure 16**). Especially, grain size and density of BCZT/0.15 ceramics are larger than that of BCZT/0.00 ceramics for each sintering temperature. It could be concluded that a small amount of ZnO nanoparticles can be improved sintering behavior.

Figure 17 presents the comparison of the piezoelectric parameters for BCZT/0.00 and BCZT/0.15 materials. As the sintering temperature rises, the

T (°C)	1300		1350		1400		1450	
Material	**BCZT/0.15**	**BCZT/0.00**	**BCZT/0.15**	**BCZT/0.00**	**BCZT/0.15**	**BCZT/0.00**	**BCZT/0.15**	**BCZT/0.00**
G (μm)	18.2	9.7	21.6	12.1	31.4	28.5	34.6	32.4
ρ (g/cm^3)	5.52	5.01	5.60	5.31	5.64	5.57	5.69	5.62

Table 2.
Grain size, G, and density, ρ, for BCZT and BCZT/0.15 ceramics sintered at different temperatures.

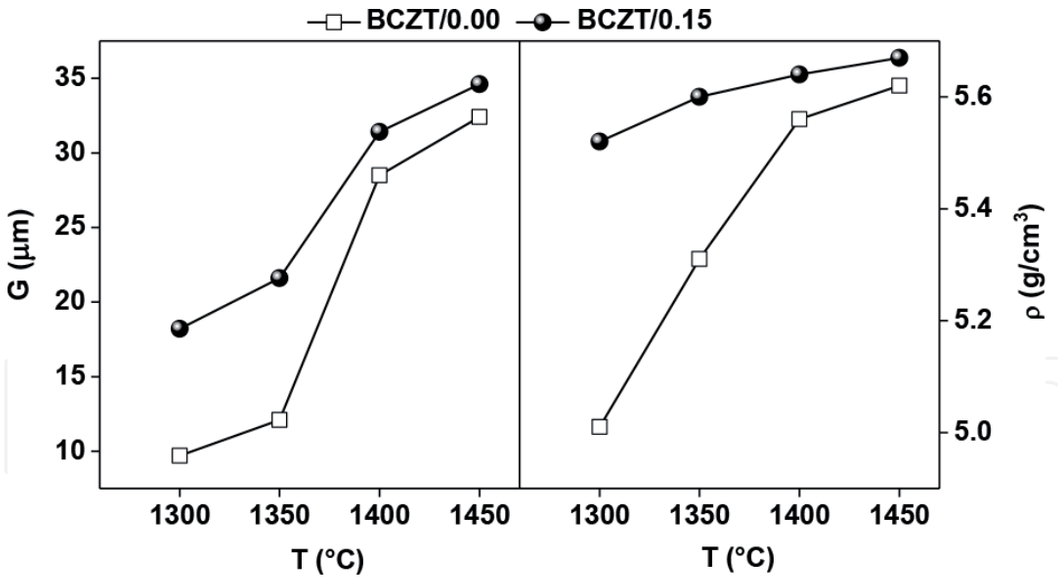

Figure 16.
Grain size and density of BCZT/0.00 and BCZT/0.15 materials as a function sintering temperature.

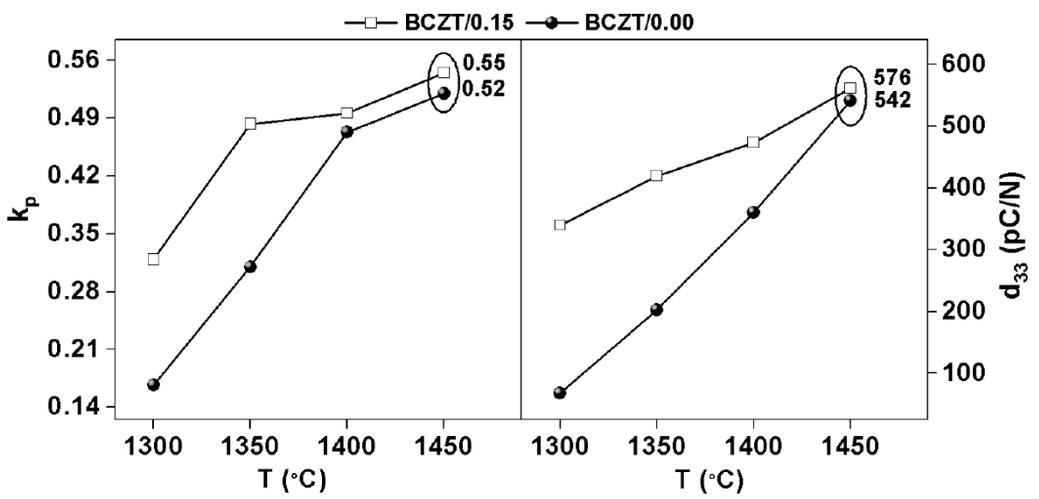

Figure 17.
Electromechanical factor, k_p, and piezoelectric coefficient, d_{33}, of BCZT/0.00 and BCZT/0.15 materials as a function sintering temperature.

piezoelectric parameters of both samples increase. Moreover, the piezoelectric parameters of BCZT/0.15 samples are higher than the ones of BCZT materials. These results may be due to the improvement in microstructure of the materials.

For the materials sintered at 1450°C, d_{33} = 576 pC/N and k_p = 0.55 were obtained for BCZT/0.15 system, whereas these parameters for BCZT/0.00 system were 542 pC/N and 0.52, respectively [9]. As known, in the MPB region, there are 14 possible polar directions with the low potential energy barrier that includes 6 in tetragonal phase and 8 in rhombohedral phase [27]. These polar directions are the optimum orientation during polarization process leading to the excellent piezoelectric properties. It could be supposed that there are only tetragonal and rhombohedral phases in two mentioning compositions and then their volume fractions are quantified as in **Table 3**. It can be seen that the nanostructured ZnO addition has heightened concentration of rhombohedral phase leading to enhance directional ability for polarization vectors. It is believed that it was the reason for the higher piezoelectric properties of BCZT/0.15 material than the BCZT/0.00 one. In other words, a competition between

Material	Tetragonal volume fraction	Rhombohedral volume fraction
BCZT/0.15	63.7%	36.3%
BCZT/0.00	71.7%	29.3%

Table 3.
Volume fraction of tetragonal and rhombohedral phases for BCZT and BCZT/0.15 materials sintered at 1450°C calculated by Eqs. (1) and (2).

structure phases with addition of ZnO nanoparticles could induce the difference in piezoelectric response for BCZT/0.00 and BCZT/0.15 samples.

4. Conclusion

The addition of ZnO nanoparticles with grain size of 59 nm has aided to successfully synthesize the BCZT/x ceramics at a relatively low sintering temperature of 1350°C. The added ZnO particles in nanoscale influenced the relaxor ferroelectric phase change of the materials. As a result, BCZT/0.15 composition possessed the highest diffuseness characteristic. Remanent polarization was improved and reached to a maximum value of 6.19 μC/cm^2 at x = 0.15, whereas the coercive field went up continuously under increasing doping concentration. The ZnO addition has also improved the quality of the piezoelectric material, and best quality was observed for BCZT/0.15 composition, given that the values of d_{33}, d_{31}, k_p, k_t, and k_{33} are 420, −174, 0.483, 0.423, and 0.571 pC/N, respectively. The obtained results suggested that the lead-free BCZT/x material could be an expected lead-free piezoelectric ceramic for applications.

Besides, the influence of sintering temperature on structure, microstructure, and some piezoelectric parameters of BCZT/0.15 sample was examined. As the sintering temperature increased, improved sintering behavior and very high piezoelectric properties of d_{33} = 576 pC/N and k_p = 0.55 were obtained for the sample sintered at 1450°C. As a comparison, corresponded properties of BCZT without ZnO nanoparticles or BCZT/0.00 specimen were investigated. The received results show that sintering behavior and some piezo-parameters of BCZT/0.15 samples are better than that of BCZT/0.00 samples at each sintering temperature. Especially, the difference in properties for samples sintered at 1450°C is attributed to competition between structure phases occurred in materials.

Acknowledgements

This work was carried out in the framework of the National Project in Physics Program until 2020 under no. ĐTĐLCN.10/18.

Author details

Dang Anh Tuan[1], Vo Thanh Tung[2*], Le Tran Uyen Tu[2] and Truong Van Chuong[2]

1 Ha Nam Provincial Department of Science and Technology, Vietnam

2 University of Sciences, Hue University, Vietnam

*Address all correspondence to: vttung@hueuni.edu.vn

References

[1] Panda PK. Review: Environmental friendly lead-free piezoelectric materials. Journal of Materials Science. 2009;**44**:5049-5062. DOI: 10.1007/s10853-009-3643-0

[2] Rodel J, Wook J, Seifert KTP, Eva-Maria A, Granzow T, Damjanovic D. Perspective on the development of lead free piezoceramics. Journal of the American Ceramic Society. 2009;**92**(6):1153-1177. DOI: 10.1111/j.1551-2916.2009.03061.x

[3] Wenfeng L, Xiaobing R. Large piezoelectric effect in Pb-free ceramics. Physical Review Letters. 2009;**103**:257602-257605. DOI: 10.1103/PhysRevLett.103.257602

[4] Xue D, Zhou Y, Bao H, Zhou C, Gao J, et al. Elastic, piezoelectric, and dielectric proper ties of $Ba(Zr_{0.2}Ti_{0.8})O_3$-$50(Ba_{0.7}Ca_{0.3})TiO_3$ Pb-free ceramic at the morphotropic phase boundary. Journal of Applied Physics. 2011;**109**:054110. DOI: 10.1063/1.3549173

[5] Damjanovic D, Biancoli A, Batooli L, Vahabzadeh A, Trodahl J. Elastic, dielectric, and piezoelectric anomalies and Raman spectroscopy of $0.5Ba(Ti_{0.8}Zr_{0.2})O_3$-$0.5(Ba_{0.7}Ca_{0.3})TiO_3$. Applied Physics Letters. 2012;**100**:192907. DOI: 10.1063/1.4714703

[6] Wu J, Xiao D, Wu W, Chen Q, Zhu J, Yang Z, et al. Composition and poling condition-induced electrical behavior of $(Ba_{0.85}Ca_{0.15})(Ti_{1-x}Zr_x)O_3$ lead-free piezoelectric ceramics. Journal of the European Ceramic Society. 2012;**32**:891-898. DOI: 10.1016/j.jeurceramsoc.2011.11.003

[7] Wang P, Li Y, Lu Y. Enhanced piezoelectric properties of $(Ba_{0.85}Ca_{0.15})(Ti_{0.9}Zr_{0.1})O_3$ lead-free ceramics by optimizing calcinations and sintering temperature. Journal of the European Ceramic Society. 2011;**31**:2005-2012. DOI: 10.1016/j.jeurceramsoc.2011.04.023

[8] Su S, Zuo R, Lu S, Xu Z, Wang X, Li L. Poling dependence and stability of piezoelectric properties of $Ba(Zr_{0.2}Ti_{0.8})O_3$-$(Ba_{0.7}Ca_{0.3})TiO_3$ ceramics with huge piezoelectric coefficients. Current Applied Physics. 2011;**11**:S120-S123. DOI: 10.1016/j.cap.2011.01.034

[9] Tuan DA, Tinh NT, Tung VT, Chuong TV. Ferroelectric and piezoelectric properties of lead-free BCT- xBZT solid solutions. Materials Transactions. 2015;**56**(9):1370-1373. DOI: 10.2320/matertrans.MA201511

[10] Dung QTL, Chuong VT, Anh PD. The effect of TiO_2 nanotubes on the sintering behavior and properties of PZT ceramics. Advances in Natural Sciences: Nanoscience and Nanotechnology. 2011;**2**:025013. DOI: 10.1088/2043-6262/2/2/025013

[11] Hayati R, Barzegar A. Microstructure and electrical properties of lead free potassium sodium niobate piezoceramics with nano additive. Materials Science and Engineering B. 2010;**172**:121-126. DOI: 10.1016/j.mseb.2010.04.033

[12] Ying-Chieh L, Tai-Kuang L, Jhen-Hau J. Piezoelectric properties and microstructures of ZnO-doped $Bi_{0.5}Na_{0.5}TiO_3$ ceramics. Journal of the European Ceramic Society. 2011;**31**:3145-3152. DOI: 10.1016/j.jeurceramsoc.2011.05.010

[13] Ramajo LA, Taub J, Castro MS. Effect of ZnO addition on the structure, microstructure and dielectric and piezoelectric properties of $K_{0.5}Na_{0.5}NbO_3$ ceramics. Materials Research. 2014;**17**(3):728-733. DOI: 10.1590/S1516-14392014005000048

[14] Saeri MR, Barzegar A, Moghadama HA. Investigation of nano particle additives on lithium doped KNN lead free piezoelectric ceramics. Ceramics International. 2011;**37**(8):3083-3087. DOI: 10.1016/j.ceramint.2011.05.044

[15] Bari AR et al. Effect of solvent on the particle morphology of nanostructured ZnO. Indian Journal of Pure and Applied Physics. 2009;**47**:24-27

[16] Yingying L, Leshu Y, Heyong H, Yuying F, Dongzhen C, Xin X. Application of the soluble salt-assisted route to scalable synthesis of ZnO nanopowder with repeated photocatalytic activity. Nanotechnology. 2012;**23**(6):065402-065409. DOI: 10.1088/0957-4484/23/6/065402

[17] Quintana-Nedelcos A, Fundora A, Amorín H, Siqueiros JM. Effects of Mg addition on phase transition and dielectric properties of $Ba(Zr_{0.05}Ti_{0.95})O_3$ system. The Open Condensed Matter Physics Journal. 2009;**2**:1-8. DOI: 10.2174/1874186X00902010001

[18] Kraus W, Nolze G. POWDER CELL - a program for the representation and manipulation of crystal structures and calculation of the resulting X-ray powder patterns. Journal of Applied Crystallography. 1996;**29**:301-303. DOI: 10.1107/S0021889895014920

[19] Tuan DA, Tung VT, Phuong LV. Analyzing 2D structure images of piezoelectric ceramics using ImageJ. International Journal of Materials and Chemistry. 2014;**4**(4): 88-91. DOI: 10.5923/j.ijmc.20140404.02

[20] The Institute of Electrical and Electronics Engineers, Inc. IEEE Standard on Piezoelectricity, ANSI/IEEE Std 176-1987

[21] Gao J, Xue D, Wang Y, Wang D, Zhang L, Wu H, et al. Microstructure basis for strong piezoelectricity in Pb-free $Ba(Zr_{0.2}Ti_{0.8})O_3$-$(Ba_{0.7}Ca_{0.3})TiO_3$ ceramics. Applied Physics Letters. 2011;**99**:092901. DOI: 10.1063/1.3629784

[22] Hao J, Bai W, Li W, Zhai J. Correlation between the microstructure and electrical properties in high-performance $(Ba_{0.85}Ca_{0.15})(Zr_{0.1}Ti_{0.9})O_3$ lead-free piezoelectric ceramics. Journal of the American Ceramic Society. 2012;**95**(6):1998. DOI: 10.1111/j.1551-2916.2012.05146.x

[23] Dobal PS, Dixit A, Katiyar RS. Effect of lanthanum substitution on the Raman spectra of barium titanate thin films. Journal of Raman Spectroscopy. 2007;**38**:142-146. DOI: 10.1002/jrs.1600

[24] Mudinepalli VR, Feng L, Wen-Chin L, Murty BS. Effect of grain size on dielectric and ferroelectric properties of nanostructured $Ba_{0.8}Sr_{0.2}TiO_3$ ceramics. Journal of Advanced Ceramics. 2015;**4**(1):46-53. DOI: 10.1007/s40145-015-0130-8

[25] Wu J, Xiao D, Wu W, Chen Q, Zhu J, Yang Z, et al. Role of room-temperature phase transition in the electrical properties of (Ba, Ca)(Ti, Zr)O_3 ceramics. Scripta Materialia. 2011;**65**:771-774. DOI: 10.1016/j.scriptamat.2011.07.028

[26] Tuan AD, Tung TV, Chuong VT, Tinh TN, Huong TMN. Structure, microstructure and dielectric properties of lead-free BCT-xBZT ceramics near the morphotropic phase boundary. Indian Journal of Pure and Applied Physics. 2015;**53**:409-415

[27] Shrout TR, Zhang SJ. Lead-free piezoelectric ceramics: Alternatives for PZT? Journal of Electroceramics. 2007;**19**:111-124. DOI: 10.1007/s10832-007-9047-0